estec

European Space Research
and Technology Centre
Keplerlaan 1
2201 AZ Noordwijk
The Netherlands
Tel. (31) 71 5656565
Fax (31) 71 5656040
www.esa.int

DOCUMENT

Correcting for Stellar Activity

Document leads: Ignasi Ribas, Giusi Micela and Giovanna Tinetti, with contributions from Enrique Herrero and Camilla Danielski

Prepared by Ignasi Ribas, Giusi Micela, Giovanna Tinetti, with contributions from Enrique Herrero and Camilla Danielski, and the EChO SST
Reference EChO-PhaseA-SRE-SA-002
Issue 2
Revision 0
Date of Issue 16th December, 2013
Status
Document Type
Distribution

European Space Agency
Agence spatiale européenne

APPROVAL

Title Correcting for stellar activity	
Issue 2	**Revision 0**
Author Ignasi Ribas, Giusi Micela, Giovanna Tinetti and the EChO SST	**Date 16/12/2013**
Approved by	**Date**

CHANGE LOG

Reason for change	Issue	Revision	Date
Update of document prior to end of Phase A study	2	0	13/12/2013

CHANGE RECORD

Issue	Revision		
Reason for change	**Date**	**Pages**	**Paragraph(s)**

Table of contents:

1 INTRODUCTION

Stellar activity in late-type main sequence stars induces photometric modulations and apparent radial velocity variations that may hamper the detection of Earth-like planets and the measurement of their transit parameters (Barros et al. 2013), mass and atmospheric properties. A tacit assumption of the EChO observing model is that any temporal variation in the calibrated signal from the (unresolved) host star/exoplanet can be attributed to changes in the (small) signal from the exoplanet, and is not a result of variation in either the stellar signal or instrument response.

Late-type stars (i.e., late-F, G, K and M spectral types) are known to be variable to some extent. The effect of stellar activity in the photosphere is seen in the form of spots and faculae, whose relationship with stellar parameters such as mass and age is still not well understood. The signal of these activity patterns is modulated by the stellar rotation period, usually producing a clear peak in the flux power spectrum of the star. The evolution of active regions, characterized by their lifetime and typical size or filling factor, has also been the subject of study of several recent works involving different methods for modelling data from spotted stars (Lanza et al. 2003; Kipping 2012). Also other phenomena exist which may induce periodic signals in photometric and radial velocity data. Pulsations, granulation, evolution of active regions and magnetic cycles may limit the capabilities of some planet searches to success and need to be subtracted or accounted for the design of searching strategies (Dumusque et al. 2011a, 2011b; Moulds et al. 2013).

The most up-to-date and comprehensive information on stellar variability comes from the studies with Kepler (stability of 200/40 ppm in a 6.5 hr period on a 11/7 mag (V) star) that are based on the observation and analysis of ~150,000 stars taken from the first Kepler data release. Ciardi et al (2011) [RD6] have found that 80% of M dwarfs have dispersion less than 500 ppm over a period of 12 hours, while G dwarfs are the most stable group down to 40 ppm. Kepler operates in the visible (430 – 890 nanometer) where stellar photometric variability is a factor of more than 2 higher than in the “sweet spot” of EChO – the near and thermal IR – due to increasing contrast between spots and the stellar photosphere with decreasing wavelength. Timescales for stellar activity are mostly very different from those associated with single transit observations (a few hours) and so removal of this spectral variability is possible. As a case in point, photometric modulations in the host of CoRoT-7 b are of the order of 2% and yet a transit with a depth of 0.03% was identified. Analyses of observations from Kepler have yielded comparable results. Note that the timescale for phase variation and stellar variability is more similar.

The effects of stellar activity on EChO are very different in the case of primary (transit) and occultation observations. Alterations in the spot distribution across the stellar surface can modify the transit depth (because of the changing ratio of photosphere and spotted areas on the face of the star) when multiple transit observations are considered, potentially giving rise to spurious planetary radius variations. Correction of this effect requires the use of very quiet stars or precise modelling of the stellar surface using external constraints. The

situation is much simpler for occultations, where the planetary emission follows directly from the depth measurement. In this case, only activity-induced variations on the timescale of the duration of the occultation need to be corrected for to ensure that the proper stellar flux baseline is used. In the particular case of EChO, photometric monitoring in the visible will aid in the correction of activity effects in the near and thermal IR.

In this document we provide details on how stellar activity will be dealt with in the framework of EChO. These methodologies developed to correct EChO data for the effects of stellar activity are presented and discussed in Sections 2 (direct scaling of activity signals), 3 (spectral shaphe in the visible), and 4 (non-parametric approach).

2 CORRECTING ECHO DATA FOR STELLAR ACTIVITY BY DIRECT SCALING OF ACTIVITY SIGNALS

2.1 Simulation of the photosphere of active stars

A methodology to simulate spectra from the spotted photosphere of a rotating star has been developed. We use atmosphere models for low mass stars to generate synthetic spectra for the stellar surface, spots and faculae. The spectrum of the entire visible face of the star is obtained by summing the contribution of a grid of small surface elements and by considering their individual Doppler shift, area of the surface element, projection angle and limb darkening. Using such simulator, time series spectra can be obtained covering the rotation period the star or longer. By convolving these with the known bandpass for a specific instrument, they can be used to study the chromatic effects of spots and faculae on photometric modulation and radial velocity jitter.

Among the most recent model atmosphere grids, we use spectra from the BT-Settl database (Allard et al. 2013) generated with the Phoenix code in order to reproduce the spectral signal for the different elements in the photosphere. These models include revised solar oxygen abundances and cloud model, which allow reproducing the photometric and spectroscopic properties also in very low mass stars. In our simulations of spotted stars, LTE models are used both for the quiet photosphere and the active regions (spots and faculae). Non-LTE models from Fontenla et al. (2009) are to be considered in order to model faculae in future versions of the code. BT-Settl models are available at resolutions defined by a sampling ≥0.05 Å, for 2600 K < T_{eff} < 70000 K, and several values of alpha enhancement and metallicity. An example for a solar-type star is shown in Fig. 1.

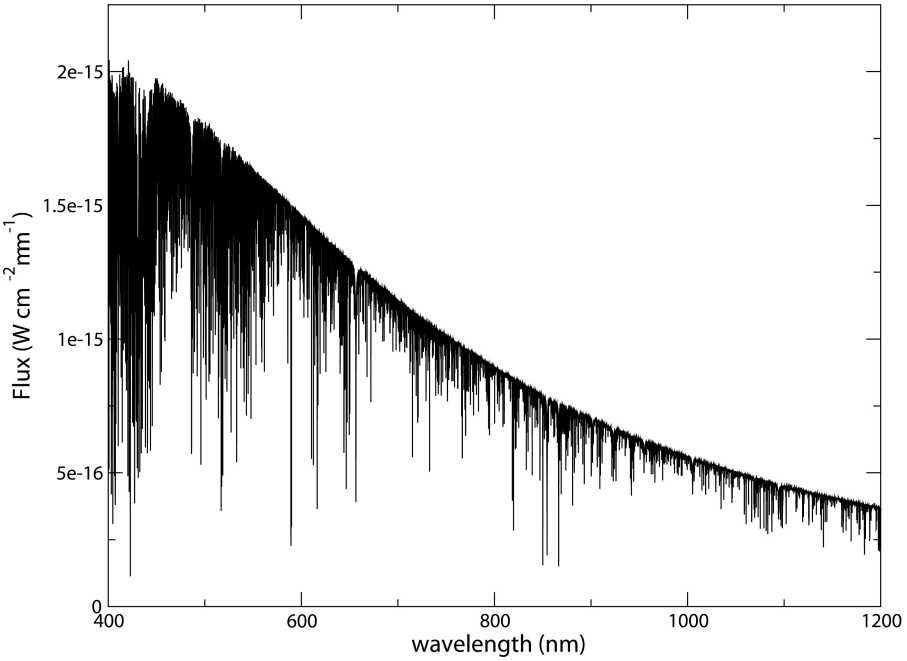

Figure 1: Spectrum of a Sun-like star (T_{eff}=6000 K, log g = 4.9) generated from BT-Settl models.

The stellar photosphere is divided into a grid of surface elements. The spatial resolution of the grid is a parameter, and 1º×1º size elements have been tested to correctly reproduce most active region configurations and transiting planet effects. Three models with different temperatures are considered in order to build the stellar spectrum: quiet photosphere, spots and faculae. The spot map is specified as a list of coordinates and radii describing each active region. Individual sizes are considered, but the same temperature contrast for both spots and faculae is assumed for all the active regions, as well as the same facula-to-spot area ratio (Q). Active region evolution (i.e., rise and decay over time) is currently not implemented in the models but it will eventually be. Each active region n is modeled as a circular spot of radius R_{Sn} surrounded by a facula with a coronal shape, having an external of radius $R_{Fn} = \sqrt{Q+1} \cdot R_{Sn}$ (see Fig. 2).

The differential rotation of the star is modeled considering:

$$P(\phi) = P_0 + k \cdot P_{sun} \cdot \sin^2 \phi, \qquad P_{sun} = 3.1913° day^{-1}$$

where the equatorial rotation period P_o and the differential rotation factor k are specified as input parameters, and ϕ is the variable denoting the latitude. Also, the inclination of the stellar axis towards the observer is a parameter and can vary from 0º to 90º.

One or more transiting planets can be introduced in the simulations. The photometric signal for the primary transit is generated from the planet size, the ephemeris and the orbit orientation (inclination and spin-orbit angles). Eccentricity is considered to be zero in all cases.

Together with the physical parameters of the star-planet system, the spectral range for the output data, and the time span and cadence of the data series can be adjusted. The program also creates a light curve by convolving each created spectrum with a filter bandpass specified from a database. Also, a filter with a flat transfer function can be created and used to study the photometric signal at a specific wavelength range. Finally, the integration time, the telescope collecting area and the response of the detector needs to be specified in order to apply photon noise statistics to the resulting fluxes.

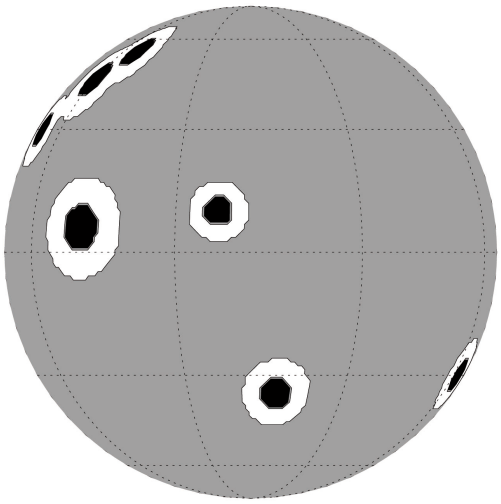

Figure 2: Projected map for an arbitrarily generated distribution of active regions. The quiet photosphere is represented in grey, and each active region is modeled as a cold spot (black) and a hotter surrounding area to account for faculae (white).

The program reads the physical parameters for the three photospheric features of the modeled star (quiet photosphere, spots and faculae) and interpolates within the corresponding model grids to generate the three synthetic spectra: $f_p(\lambda)$, $f_s(\lambda)$ and $f_f(\lambda)$. Also, Kurucz (ATLAS9) spectra are generated for the same parameters for the photosphere, spots and faculae, as these models provide information on the limb darkening profile function $I(\lambda,\mu)/I(\lambda,0)$.

First, the spectrum for an immaculate photosphere is obtained from the contribution of all the surface elements, taking into account the geometry of the element, its projection towards the observer, its limb darkening function and its radial velocity shift:

$$f_{im}(\lambda+\Delta\lambda)=\sum_k f_p(\lambda,\mu_k,a_k)=\sum_k f_p(\lambda)\otimes\frac{I_p(\lambda,\mu_k)}{I_p(\lambda,0)}\cdot a_k\cdot\mu_k\cdot\omega_k,$$

where k is the surface element and μ_k is its projection angle given by

$$\mu_k=\sin i\sin\theta_k\cos\phi_k+\cos i\cos\theta_k.$$

The factor ω_k accounts for the visibility of the surface element and is given by

$$\omega_k=\begin{cases}1 & if\ \mu_k\geq 0\\ 0 & if\ \mu_k<0\end{cases},$$

and a_k is the area of the surface element, which can be computed from their resolution of the grid ($\Delta\alpha$) by

$$a_k = 2 \cdot \Delta\alpha \cdot \sin\left(\frac{\Delta\alpha}{2}\right) \sin\theta .$$

Finally, Δλ are the Doppler shifts added to the wavelength vector,

$$\Delta\lambda = -8.05 \cdot \lambda \cdot \frac{1}{c} \cdot R_{star} \cdot \frac{2\pi}{P_{rot}} \sin i \sin\theta \sin\phi .$$

with R_{star} given in R_{Sun} units. These are computed from the rotation period given in the input parameters and the stellar radius calculated using its relation with log g and T_{eff}.

The flux variations produced by the visible active regions are added to the contribution of the immaculate photosphere when computing the spectrum at each time step j. These are given by

$$\Delta f_j^{ar}(\lambda + \Delta\lambda) = \sum_k \left[\left(f_s(\lambda) - f_p(\lambda)\right) \otimes \frac{I_s(\lambda, \mu_{kj})}{I_s(\lambda, 0)} \cdot a_k \cdot \mu_{kj} \cdot \omega_k \cdot p_{kj}^s + \left(f_f(\lambda) - f_p(\lambda)\right) \cdot c_f(\mu_{kj}) \cdot a_k \cdot \mu_{kj} \cdot \omega_k \cdot p_{kj}^f \right],$$

where the first term accounts for the flux deficit produced by the spots and the second is the overflux introduced by faculae. The factors p^s_{kj} and p^f_{kj} are the fractions of the surface element k covered by spot and facula, respectively. These amounts are calculated for every surface element considering their distance to the center of all the near active regions at each observation j. There is also a time dependece of the projection of the surface elements, given by

$$\mu_k = \sin i \sin\theta_k \cos\left[\phi_k + \omega(t_j - t_0)\right] + \cos i \cos\theta_k ,$$

Finally, $c_f(\mu_k)$ accounts for the limb brightening of faculae, which is considered with a linear model:

$$c_f(\mu_k) = \chi_f(1 - \mu_k).$$

The linear coefficient χ_f is computed for the given stellar parameters, fixing that active regions (considering spots and faculae) are ~1.2 times brighter at the limb than at the center of the stellar disk (Ortiz et al. 2002; Ball et al. 2011).

Each transiting planet is considered as a dark circular spot with a fixed radius (no atmosphere) crossing the stellar disk. For each time step j, the planet position is obtained from the given ephemeris and the flux deficit is computed from the oculted surface elements of the star:

$$\Delta f_j^{tr}(\lambda + \Delta\lambda) = -\sum_k f_p(\lambda) \otimes \frac{I_s(\lambda, \mu_{kj})}{I_s(\lambda, 0)} \cdot a_k \cdot \mu_{kj} \cdot \omega_k \cdot p_{kj}^{tr},$$

where p^{tr}_{kj} is the fraction of the surface element k covered by the planet.

Finally, the spectrum for the observation j is obtained by adding the contribution of the immaculate photosphere, the active regions and the transiting planet:

$$f^j(\lambda) = f_{im}(\lambda) + \Delta f_j^{ar}(\lambda) + \Delta f_j^{tr}(\lambda)$$

When working with the low resolution spectra, the resulting time series flux vectors are convolved with the specified filter bandpass (see Fig. 3) in order to obtain the photometric jitter produced by activity at the desired spectral ranges.

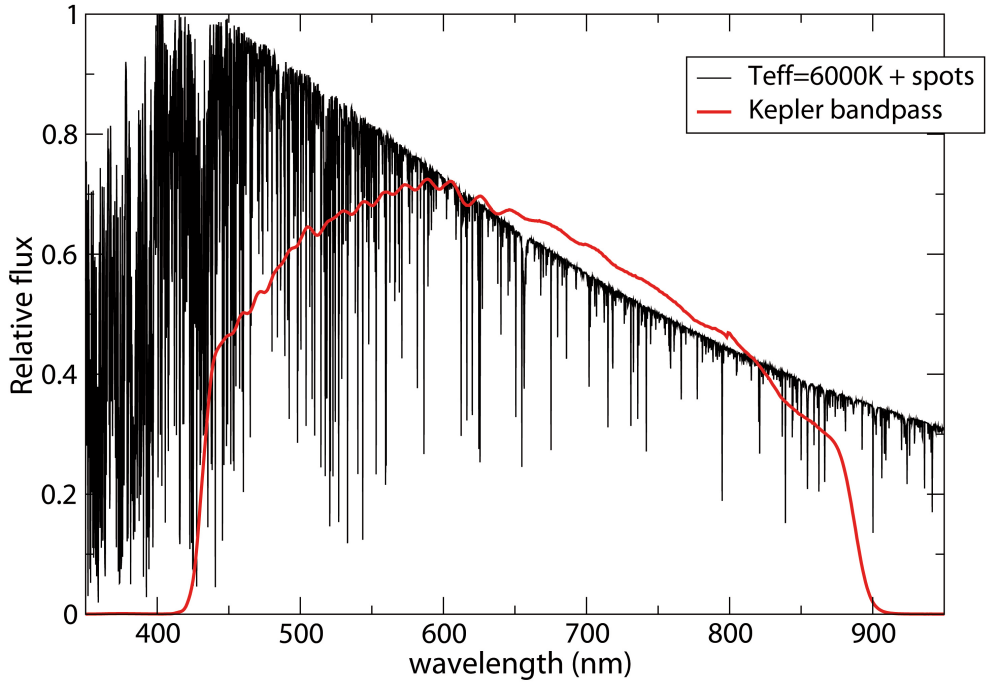

Figure 3: Normalized flux for a simulated spectrum of a G-type star with several active regions generated from BT-Settl model spectra (black). In red, the transmission function of the Kepler filter.

2.2 Full light curve scaling

The methodology described in Section 2.1 has been used to generate time series data to perform several tests for EChO data-type optimization. The simulator allows us to cover a broad spectral range including both the visible and the near-IR, so that we can accurately analyse and compare activity photometric signal amplitudes and patterns at different wavelengths and spectral resolutions.

We have considered a number of combinations of stellar photospheres and active region parameters (size and location of spots, temperature contrast) to obtain a better statistical view of the results. The process was performed for 11 cases of star-planet systems randomly selected from a set of 6 stellar models (Teff= 6200 K, 5850 K, 5060 K, 4060 K, 3580 K) having four different possible active region maps (spot locations, sizes, temperature

contrasts) and a rotation period of 15 days. The spot temperature contrast was scaled with temperature according to Berdyugina et al. (2005) and the planet parameters were fixed in all cases to R_p=0.05 R_{star}, P_{planet}=2.54 days, b=0.2 (impact parameter). The facula temperature contrast and the facula-to-spot area ratio (Q) were fixed in all cases to ΔT_{fac}=+100K and Q=7.0, respectively. Narrow bandpasses equivalent to a single spectral resolution element at R=300 centered at 0.8 μm, 2.5 μm and 5.0 μm were used in order to generate light curves of the spotted rotating stars.

The approach we have investigated to correct near IR time series data for stellar activity is based on scaling the higher-amplitude optical light curve to the near-IR wavelengths and carry out a direct correction. This procedure was defined so that it could resemble a practical procedure to be used with EChO data. The detailed steps are: 1) We first normalized the fluxes and calculated the standard deviation of the optical and near-IR photometry, σ(0.8μm), σ(2.5μm) and σ(5.0μm); 2) ratios of these standard deviations (near-IR to visible), defined as $K_{2.5}$ and $K_{5.0}$, were calculated; 3) the scaling factors $K_{2.5}$ and $K_{5.0}$ were applied to the optical light curve; and 4) the final near-IR light curve was obtained from the ratio of the generated time series to the scaled optical light curve. Tests showed that the time modulation of the near-IR light curves could be largely corrected following this approach. The sequence above was both applied to the light curve without exoplanet transits and to a light curve including transits.

We evaluated the possible performance of the method in removing activity signals by comparing the resulting corrected light curve with a light curve including transits and corresponding to a star with an immaculate photosphere. This was carried out to check whether systematic effects inside the transits were left over when following the procedure. Indeed, depending on the distribution of starspots and the trajectory of the planet across the stellar disk, the depth of the transit could experience variations (which would mask or bias the measurement of the planetary atmosphere) both in the case of spot crossing events but also if only photosphere is occulted (e.g., Ballerini et al. 2012).

In our test we divided the resulting "clean" IR light curves (i.e., corrected by scaling the 0.8-μm light curve as described above) by light curves generated for an immaculate star (with no spots) for the same stellar and planet parameters. Then, data intervals of 2·T14 (i.e., twice the total duration of the transit) around the transit events were selected for analysis. The out-of-transit baseline at either side of the transit were used to fit a linear trend that was subsequently applied to the in-transit observations. This is analogous to the common procedure used to analyse and fit transit data. The standard deviations were computed for the in-transit sections of the complete data series (which includes 10 transits). The results of this set of simulations can be seen in Table 1 and Fig. 4. Table 1 shows the stellar parameters adopted and standard deviation caused by the spot modulation at 0.8 μm, 2.5 μm and 5.0 μm bandpasses. The last two columns list the standard deviation of the in-transit data at 2.5 μm and 5.0 μm after correcting for spot modulation using the procedure described above.

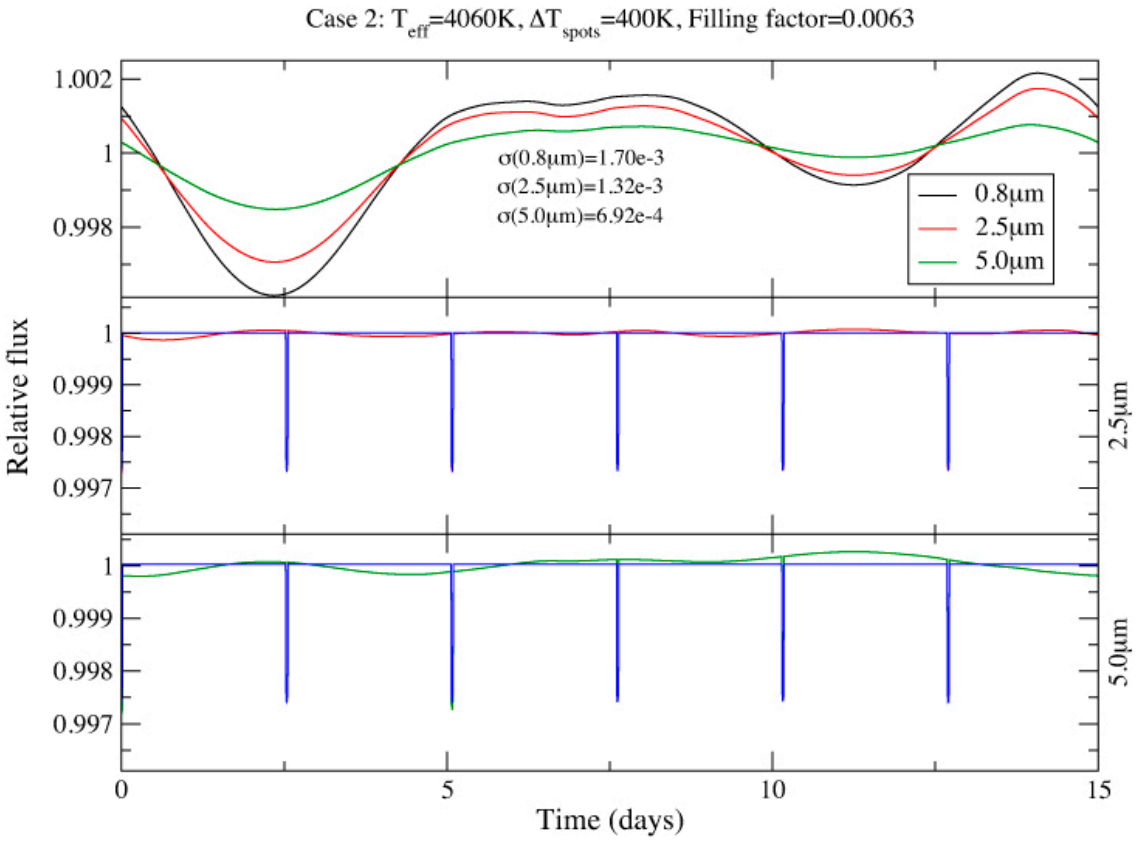

Figure 4: Top: Normalized light curves for three narrow passbands (R=300) centered at 0.8 μm (black), 2.5 μm (red) and 5.0 μm (green) for one of the cases generated in the sample. The standard deviations of the data series, used in order to compute the scale factors, are also indicated. Bottom: 2.5 μm (red) and 5.0 μm (green) light curves for the same star including a transiting planet, and corrected from the activity signal by using the scaled 0.8 μm light curve. The light curves for an immaculate star are shown in blue.

As can be seen in Table 1, most of the cases (10) that we have analysed thus far correspond to standard stars of GKM spectral types with filling factors of 0.5% to 0.9%. To define the context, our Sun ranges from filling factors of ~0% to ~0.2%. So, the stellar parameters that we have simulated correspond to stars that are some 2-3 times more active than the active Sun. According to the Kepler mission results (e.g., Basri et al. 2013), this would be representative of the 20% of the solar neighbourhood population and thus indicate a statistical upper limit to what we can expect of the exoplanet host distribution. As can be seen from Table 1, in the first 10 cases the plain direct procedure that we have used here provides a correction to the transit data to better than 10^{-4} and often as good as a few parts in 10^{-5}. Note also that, if obvious photometric outliers corresponding to spot crossing events are cleaned, the results are further improved and in all cases the residual standard deviation is below ~$1.3 \cdot 10^{-5}$.

T_{eff} (K)	ΔT_{sp} (K)	Filling factor	rms (0.8μm)	rms (2.5μm)	rms (5.0μm)	rms_T (2.5μm)	rms_T (5.0μm)	$rms_{T(corr)}$ (2.5μm)	$rms_{T(corr)}$ (5.0μm)
5850	500	0.0050	2.33e-3	7.18e-4	7.42e-4	4.52e-5	4.58e-5	1.07e-5	1.12e-5
4060	400	0.0063	1.70e-3	1.32e-3	6.92e-4	5.70e-5	2.76e-5	1.24e-5	5.25e-6
5060	500	0.0089	1.85e-3	8.97e-4	6.43e-4	3.36e-5	2.63e-5	1.01e-5	9.13e-6
3580	400	0.0077	1.75e-3	9.62e-4	3.97e-4	4.83e-5	5.04e-5	3.55e-6	4.66e-6
5850	500	0.0063	1.70e-3	9.78e-4	7.46e-4	2.99e-5	2.26e-5	6.94e-6	7.20e-6
6200	550	0.0077	9.76e-4	3.85e-4	4.06e-4	1.08e-5	1.16e-5	2.68e-6	2.77e-6
4060	400	0.0050	3.38e-3	2.56e-3	1.30e-3	1.26e-4	6.17e-5	2.08e-6	1.02e-5
4060	400	0.0077	1.35e-3	1.06e-3	5.30e-4	3.25e-5	1.56e-5	6.38e-6	3.69e-6
5850	500	0.0077	9.43e-3	4.41e-4	4.95e-4	1.30e-5	1.37e-5	1.70e-6	1.76e-6
3580	400	0.0089	2.21e-3	1.13e-3	9.35e-4	5.16e-5	3.99e-5	1.17e-5	9.01e-6
5060	500	0.0482	1.55e-2	7.09e-3	5.25e-3	1.31e-4	1.02e-4	3.53e-5	2.77e-5

Table 1: Results for the simulations of 11 cases of star-planet systems randomly selected from a set of 6 stellar models and 4 different possible active region maps, and with a rotation period of 15 days. The planet parameters were fixed to R_p=0.05 R_{star}, P_{planet}=2.54 days, b=0.2 (impact parameter). The facula temperature contrast and the facula-to-spot area ratio (Q) were fixed to ΔT_{fac}=+100 K and Q=7.0, respectively. The first three columns indicate the temperature for the quiet photosphere, the spot contrast and the spot filling factor. The following three columns list the standard deviation of the (spotted) light curves at 0.8, 2 and 5 μm. The two columns labelled rms_T show the standard deviation of the in-transit sections at 2.5 μm and 5.0 μm after correcting for activity and transit effects. The final two columns give the standard deviation of the data analysed in the previous two columns but after correcting for outliers caused by spot crossing events.

The last row of Table 1 corresponds to a rather active star with similar parameters to the explanet host HD 189733. The filling factor is around 4% and in this case the standard deviation of the 0.8, 2 and 5 μm light curves is of the order of 5-10 times greater than in the previous 10 cases. But the results show that the scaling procedure works quite efficiently in this case as well and the standard deviations of the corrected transit events is of ~$1 \cdot 10^{-4}$. The standard deviation is further reduced to ~$3 \cdot 10^{-5}$ when spot crossing outliers are cleaned.

The procedure explained here constitutes a direct methodology to correct transit data that may be the simplest approach to address stellar activity effects. Even in this case, our results show that it is possible to reach precisions better than 10^{-4} on transit data in the near IR for most of the stellar host population. If further care is taken and outliers caused by spot crossing events are cleaned, the precision reachable approaches 10^{-5} or better in most instances. This is even the case of a moderately active exoplanet host such as HD 189733. The tests that we present show that the final in-transit standard deviation is a factor 2-5·10^2 smaller than the original standard deviation of the light curve at 0.8 μm. This simple rule-of-thumb can be used to assess the maximum photometric activity tolerable to attain the precision requirements of EChO with this direct scaling technique. More strongly active targets, which may exist considering that EChO will observe M-type planet hosts, are very likely to require a more sophisticated analysis methodology in order to reach precisions in the range 10^{-4}–10^{-5}.

A shortcoming of this methodology is that it requires continuous or nearly-continuous spectrophotometry to model the out-of-transit variability and calculate the scaling factors. In the case of EChO, this may occur for some transiting planets with a vary large number of observations or may require of supporting ground-based observations to monitor the photometric variations. Given these restrictions we have explored another method to correct transit and eclipse data that does not require other observations than those of the events themselves.

2.3 VIS-IR transit depth correlations

In wiev of the need of continuous spectrophotometry to apply the methodology in 2.2, we have investigated a direct method of correlating activity-induced variations in the visible with those in the IR. The underlying hypothesis is that variations of the transit depth in the visible are solely caused by stellar activity effects and not influenced by the atmosphere of the transiting planet. The spectral signal of the planetary atmosphere in the visible is significantly weaker than in the IR and time variations should be negligible, thus lending support to the working hypothesis. In this framework, by characterizing variations in the visible it should be possible to correct out activity-induced variations in the IR.

To simulate the performance of the method we have considered a number of combinations of stellar photospheres and active region parameters (size and location of spots, temperature contrast) for a good statistical view of the results. The process was performed for 10 cases of star-planet systems randomly selected from a set of 6 stellar models (Teff= 6200 K, 5850 K, 5060 K, 4060 K, 3580 K) having four different possible active region maps (spot locations, sizes, temperature contrasts) and a rotation period of 15 days. Note that we are now considering higher filling factors than in the case of Sect. 2.2. The spot temperature contrast was scaled with temperature according to Berdyugina et al. (2005) and the planet parameters were fixed in all cases to R_p=0.05 R_{star}, P_{planet}=2.54 days, b=0.2 (impact parameter). The facula temperature contrast and the facula-to-spot area ratio (Q) were fixed in all cases to ΔT_{fac}=+100K and Q=7.0, respectively. Narrow bandpasses equivalent to a single spectral resolution element at R=300 centered at 0.8 μm, 2.5 μm and 5.0 μm were used in order to generate light curves of the spotted rotating stars, this time only in the interval around the transit events (2·T14 total width).

From the model light curve we have measured the transit depths, using common techniques, and calculated the variations of those depths with time. This was repeated for all the transit events of all our simulated cases. The combined dataset of all transit depths was then analysed for correlations. We have found that there is a well-defined correlation between activity-induced transit depth variations in the visible (0.8 μm) and the IR (2.5 and 5.0 μm). An illustration of the transit light curves generated by the simulator and the correlation between visible and IR transit depth variations (TDV) can be seen in Fig. 5, including linear regression fits.

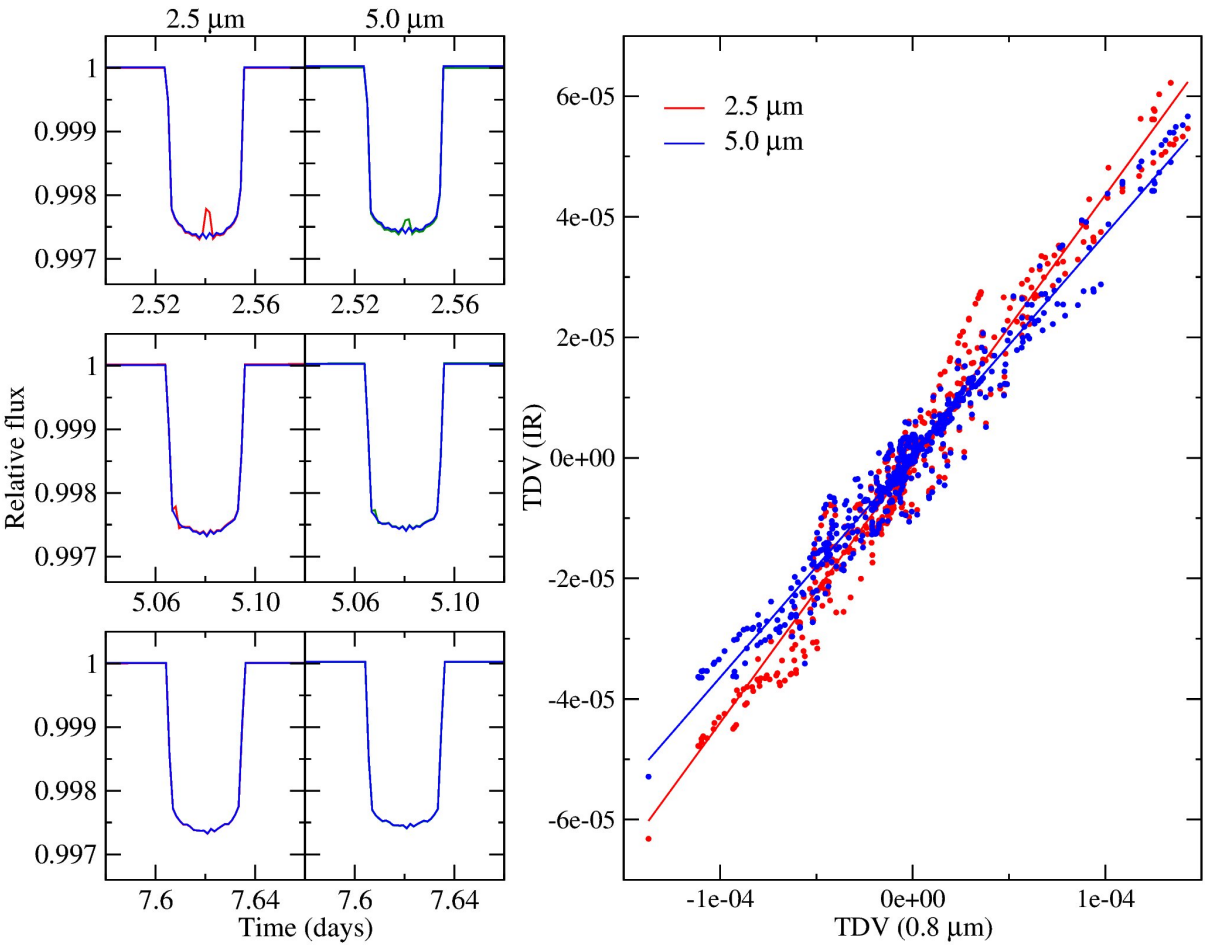

Figure 5: Left: Transit light curves at 2.5 μm (red) and 5.0 μm (green) for one of the cases generated in the sample, compared with the transit light curve of an immaculate star. Note the small systematic deviations and the more apparent spot crossing events. Right: Correlation of activity-induced transit depth variations (TDV) in the visible (0.8 μm) and the IR (2.5 and 5.0 μm).

The methodology for correcting EChO data for stellar activity effects using, for example, a series of measurements in the visible and an IR band can be carried out using the following expression:

$$d_{IR}^{corr} = d_{IR} + a_0 + a_1 \cdot (d_{VIS} - \langle d_{VIS} \rangle),$$

where d stands for the transit depth, and a_0 and a_1 are the coefficients of a linear fit that can be determined from simulations (shown in Figure 5 as an example for our simulated cases). Actually, our tests show that $a_0$takes negligible values and can be adopted as 0.

We tested the performance of the method by coming back to our simulated transit depth data. The linear regression takes values $a_1 = 0.438$ for the 2.5 μm data and $a_1 = 0.368$ for 5.0 μm. For each transit event, we used the general coefficients and the visible TDV to correct the IR depth for stellar activity. Then, we analysed the resulting scatter in the depth

variations of the combined events for each simulated case. The results can be seen in Table 2. The cases that we have analysed represent standard stars of GKM spectral types with filling factors of 1-7%, i.e., corresponding to stars that are ~4-30 times more spotted than the active Sun. The case in row 1 has parameters similar to HD 189733. As can be seen from Table 2, we start with initial transit depth rms values that are generally around 10^{-3}. Correction using the procedure described decreases such rms by factors ranging from 20 to several hundreds. Thus, the resulting rms in the transit depth variations in the IR shows that this procedure provides a correction of the transit data to a few times 10^{-5}. For more active stars (which will be a very small subsample, anyway) the correction may not reach this high performance, but the final TDV rms is very likely not to exceed 10^{-4}, and in any event stay fully compliant with EChO noise requirements.

T_{eff} (K)	ΔT_{sp} (K)	Filling Factor	rms_T (0.8μm)	rms_T (2.5μm)	rms_T (5.0μm)	$rms_{T(corr)}$ (2.5μm)	$rms_{T(corr)}$ (5.0μm)	Corr. fact (2.5μm)	Corr. fact (5.0μm)
5060	500	0.061	9.0e-3	3.9e-3	3.0e-3	1.7e-5	2.3e-5	2.3e2	1.3e2
5850	500	0.053	7.3e-3	2.9e-3	2.9e-3	4.0e-5	2.5e-5	7.3e1	1.2e2
6200	550	0.049	4.4e-3	1.7e-3	1.8e-3	5.3e-6	5.9e-6	3.2e2	3.1e2
3580	400	0.055	1.1e-2	6.2e-3	4.7e-3	3.8e-5	2.2e-5	1.6e2	2.1e2
4060	400	0.035	7.1e-3	5.3e-3	2.6e-3	4.4e-5	3.4e-6	1.2e2	7.6e2
5850	500	0.008	1.9e-4	1.4e-4	1.5e-4	8.9e-6	9.8e-6	1.6e1	1.5e1
5850	500	0.060	6.3e-3	2.6e-3	2.7e-3	3.2e-5	2.7e-5	8.1e1	1.0e2
3580	400	0.066	1.5e-2	8.3e-3	6.4e-3	3.0e-5	2.2e-5	2.8e2	2.9e2
5850	500	0.020	2.0e-3	9.2e-4	9.7e-4	1.9e-5	2.4e-5	4.8e1	4.0e1
5060	500	0.074	5.1e-3	2.2e-3	1.7e-3	1.4e-5	1.5e-5	1.6e2	1.1e2

Table 2: Results for the simulations of 10 cases of star-planet systems randomly selected from a set of 6 stellar models and 4 different possible active region maps, and with a rotation period of 15 days. The planet parameters were fixed to R_p=0.05 R_{star}, P_{planet}=2.54 days, b=0.2 (impact parameter). The facula temperature contrast and the facula-to-spot area ratio (Q) were fixed to ΔT_{fac}=+100 K and Q=7.0, respectively. The first three columns indicate the temperature for the quiet photosphere, the spot contrast and the spot filling factor. The following three columns list the rms of the in-transit sections at 0.8, 2.5, and 5.0 μm. The next two columns give the rms of the in-transit sections at 2.5 and 5.0 μm after correcting for activity effects using the procedure described in the text. The final two columns give the correction factor at 2.5 and 5.0 μm.

3 CORRECTION METHOD BASED ON SPECTRAL SHAPE IN THE VISIBLE BAND

Here we present a method to correct the stellar spectrum for activity effects that takes advantage of large simultaneous wavelength EChO coverage and moderate spectral resolution. The method uses the shape of the spectrum in the visible band to predict the shape of the spectrum in the infrared and correct it.

In order to calibrate the method we need a set of spectra covering as much as possible the entire possible activity levels; the ideal set will be given by the spectra out of transits collected by EChO itself. This will be the best data set to adapt the method to a for given star, with the reasonable assumption that stellar spectra during the transits do not behave in a different way than out of transit. The calibration will be easily refined and updated by accumulating data during the EChO lifetime.

Today we do not have EChO observed spectra, therefore we have developed and tested the method on a set of simplified models of spotted stars, but may be generalized to any kind of model or data. The only assumption behind is that the spectral variations in the NIR band are correlated to those in the visible.

Activity is prominent specially in the blue spectral window and has smaller effects (even 4-5 times smaller) in the infrared band (i.e. Ballerini et al. 2012) where the planetary signal is concentrated. We may take advantage of the broad band coverage of EChO to correct the infrared spectrum using the visible part of the spectrum. In practice we will use the visible spectrum as an instantaneous calibrator to correct the spectrum in the IR band in order to recover the planetary signal uncontaminated by stellar activity. This objective may be achieved since the spectral distortion observed in optical band may be attributed completely to the activity while the planet contribution can be neglected.

Having a sufficient number of broad band spectra of a stars observed at different levels of activity, it is possible to calibrate the technique specifically for that star. EChO will give us such spectra. In the meantime, we may develop and test the approach on models purposely built. In the following we present our models and the method of spectral correction we plan to apply to EChO spectra.

The method will be tested through simulations of a set of “real” stars with a given SNR. These “real” stars will be used to verify the capability of the method to recover the infrared spectrum, based on visible one.

3.1 Active star models

Here we simulate a set of stars at different level of activity. The model is reasonably realistic but without any claims of completeness. The aim is to enable the development and calibration of the method. While the general behavior will reflect that of the real spectra, they have no claim to reproduce the details. The model is based on the spectroscopic extension of the technique used by Ballerini et al. (2012) to estimate multi-band photometric effects of stellar activity.

Our approach to model the stellar activity is based on the assumption that activity is dominated by spots at T=T(spot) (with T(spot) < (Tstar)) covering a fraction f (filling factor) of the stellar surface.

The stellar flux in presence of spots can be expressed as in the equation below, where we are neglecting other effects, including the limb darkening (see Ballerini et al. 2012 for a discussion on these effects):

$$Flux(spotted) = Flux(star) \cdot (1 - f) + Flux(Tspot) \cdot f$$

In the following we will use flux in the [0.55 -1.0] μm band to parameterize the activity properties. The blue cutoff is imposed by the instrument requirement[1], while the red cutoff is a compromise between the need to have a band sufficiently broad and maintain as small as possible the overlap with the band "interesting" for planetary atmosphere.

For the present application for a given stellar temperature we create a grid of spotted stars as in the equation above. Flux(star) is the spectrum of the unspotted star with a temperature corresponding to the chosen spectral type. Filling factor (f) is defined in the interval f = [0.001 – 0.101] with a step of 0.001, while Flux(Tspot) is the flux at the spot temperature. We vary Tspot in the [T(star)-1500 - T(Tstar)] interval with a step of 100 K. Here we use models of Allard et al. (2013) BT- Settl (http://phoenix.ens-lyon.fr/Grids/BT-Settl/). Spectra corresponding to temperatures not present in the Phoenix library are generated interpolating spectra with the closest temperatures.

Spectra are degraded to a resolution R=300 to match the EChO resolution, filtering the original high resolution spectra with a Gaussian with □=□/300. In order to determine the principal components we use the spectral region between [0.55-1.0] μm, normalized to its integral flux since we want to detect shape variation.

3.2 Determination of principal components

The proposed method is based on principal component analysis that are linear combinations of the original variables rotated in a space of independent variables. Since the new variables are chosen with the goal to maximize the variance going from the first to the following components, it is possible, establishing a threshold to the explained variance, to reduce, even significantly, the dimensionality of the space. The technique eliminates possible dependences among the original variables and noise.

In our implementation principal components are derived centering the variables (flux in each spectral bin) to their mean.

In all explored cases two components are sufficient to explain at least 95% of the variance. The first component is directly related to the slope of the spectrum while higher order components are related to features of the spectrum. Examples of the two first components for three representative cases are reported in Fig. 6.

The two components are directly connected with the model parameters, temperature and filling factor of the spot. We show these relations for the case with T_{eff}=5250 K in Fig. 7. The two other cases present relations qualitatively similar.

[1] If the goal to achieve 0.4 μm is reached, our method will be even more effective, since activity is more prominent in the blue band.

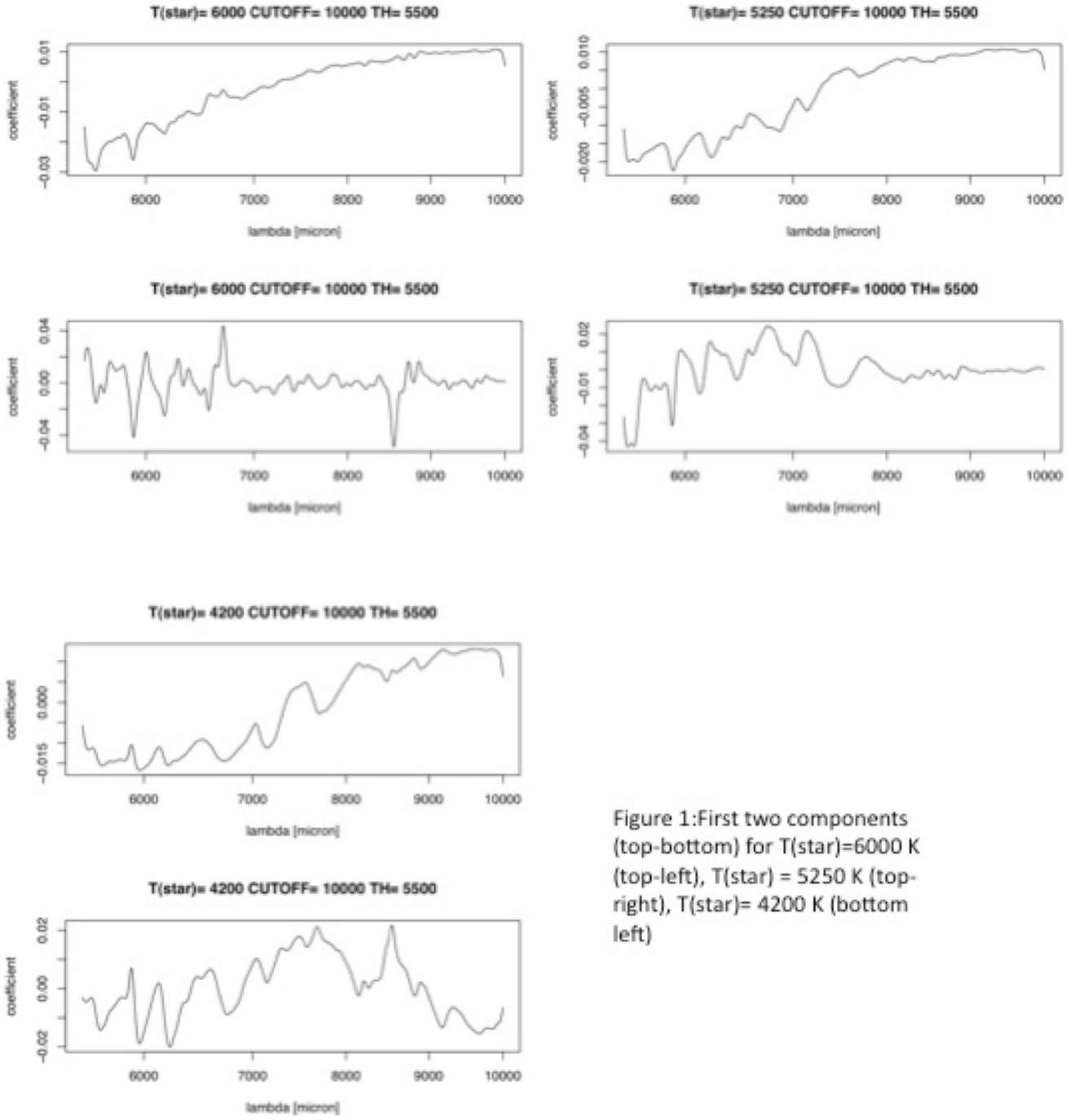

Figure 1:First two components (top-bottom) for T(star)=6000 K (top-left), T(star) = 5250 K (top-right), T(star)= 4200 K (bottom left)

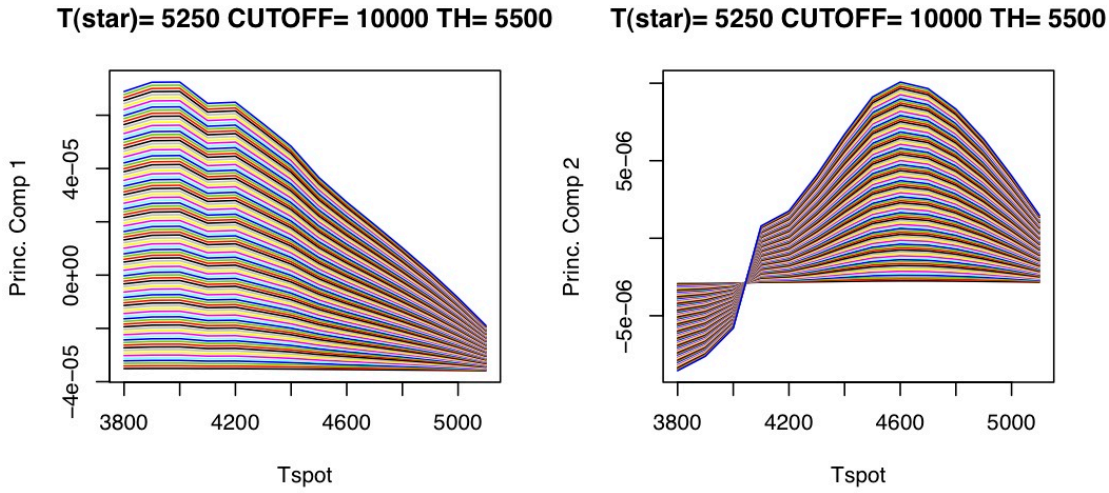

Figure 7: Dependence of first (left) and second (right) component on spot temperature for a star with T_{eff}=5250 K. Different lines correspond to different filling factors (the highest in the upper part of the plot).

The first component alone is not sufficient to determine univocally the spectral shape, here parameterized by both the spot temperature and filling factor, presenting a degeneracy in the two parameters. The combination of the first two components allows us to break this degeneracy and recover the original spectrum. By projecting an observed spectrum on the principal component space we should be able to derive the spot parameters and correct the infrared spectrum for stellar activity. The plane defined by the two components for the case with T=5250 K is shown in Figure 8.

The following analysis has been performed for stars with three representative temperatures. The adopted parameters are reported in Table 3.

	Go	**mid-G**	**K5**
T(star) (K)	6000	5250	4200
Tspot (K)	4500 - 5900	3700 - 5100	2700 - 4100
f	0.001-0.101	0.001-0.101	0.001-0.101

Table 3: Summary of parameters used to build the grid used to derive the Principal Components.

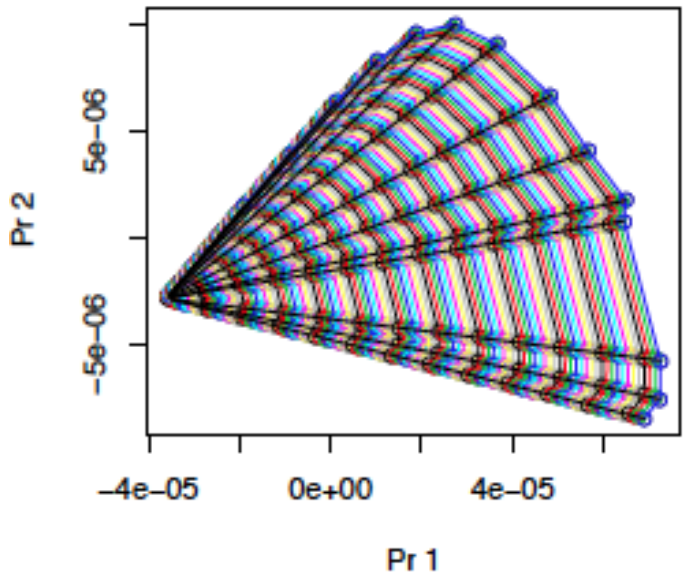

Figure 8: Relation between the two first components for the case with T(star)=5250 K. Different lines indicate different filling factors.

3.3 Simulations and spectra recovery

In order to test the method capability to recover the spot parameters we have simulated a set of representative combinations of star-spot assuming three average SNRs per resolution element in the visible band (assuming a flat spectral instrument response). For each combination we have generated 1000 simulations and projected the resulting visible spectra in the space defined by the first two principal components. In order to recover the input spectrum we do not perform a fit, but chose the closest point of the grid, therefore our sensitivity is limited by the resolution of the grid itself: Δf=0.001 and ΔT=100 K, respectively. Of course a more sophisticated fitting procedure may be performed to obtain a finer tuning of the procedure.

After identifying the "best fitted" visible spectrum we adopt the corresponding NIR spectrum as the best estimate of the observed spectrum, corrected for the activity effect.

For each of the tested case the procedure includes the following steps:

- Generation of 1000 simulations of the input model assuming a given average SNR per resolution element;
- Projection of the simulated spectra (in the visible band) on the space determined by the first two components identified above;

- Identification of the "best fitted spectrum" among those present in the grid in the principal component space, and choice of the corresponding NIR spectrum as the "best estimate" of the NIR stellar spectrum
- Comparison of the residual spectral distortion without any corrections (assuming an unspotted star) and after adopting the best estimate

We tested this method on a few representative cases: stars with T_{eff}=6000, 5200, 4200 K, respectively; ΔT=700 K; f=0.01, for three different average signal to noise: 200, 500, 1000. SNR=200 is the minimum value allowed by the EChO scientific requirements, while the latter two SNRs correspond to more realistic values obtained by EChOSim and the radiative model for transit spectroscopy of known planets. Fig. 9 shows the results, comparing the spectral distortion without any correction (black line) and the residual distortion after correcting with the best estimate. The figure reports the median correction of the distribution of the 1000 simulations and the 25 and 75% quantiles to give an estimate of the uncertainty of the correction for the three adopted SNRs. To quantify the correction we compare the original distortion before applying our method, measured as the average value in the 1-2 μm band (where the effect is larger) and the equivalent average on the median and 25-75% quantiles of the residual distortion after correcting. This comparison is shown in Table 4. We see that, on average, the method works well allowing us a significant reduction of the spectral distortion. Photon noise may produce a larger residual on a single measurement (as measured by percentiles), in particular for latest types. However we note that for targets at the lowest SNR we expect to observe many transits, therefore also in these cases, on average, the stellar activity will be significantly corrected. On the contrary targets requiring few transits will be typically observed at high SNR, where the individual correction are good also for individual simulations.

		Residual distortion after correcting		
Teff [K]	**No correction (average 1-2 μm)**	**SNR=200 (±25-75% quartiles)**	**SNR=500 (±25-75% quartiles)**	**SNR=1000 (±25-75% quartiles)**
6000	2.2e-3	-6.4e-5 [-9e-4 / 7e-4]	8.6e-5 [-5e-4 / 4e-4]	1.2e-4 [-4e-4 / 4e4]
5200	2.5e-3	-2.9e-4 [-1e-3 / 3e-4]	-6.8e-5 [-5e-4 / 2e-4]	5.2e-5 [-2e-4 / 2e-4]
4200	4.8e-3	3.0e-6 [-2e-3 / 1e-3]	4.0e-6 [-1e-3 / 9e-4]	0 [-3.8e-4 / 5e-4]

Table 4: Comparison between spectral distortion without any corrections and the residual after correcting, as a function of stellar effective temperature and SNR. We report the average values and the 25-75% percentiles derived from 1000 simulations.

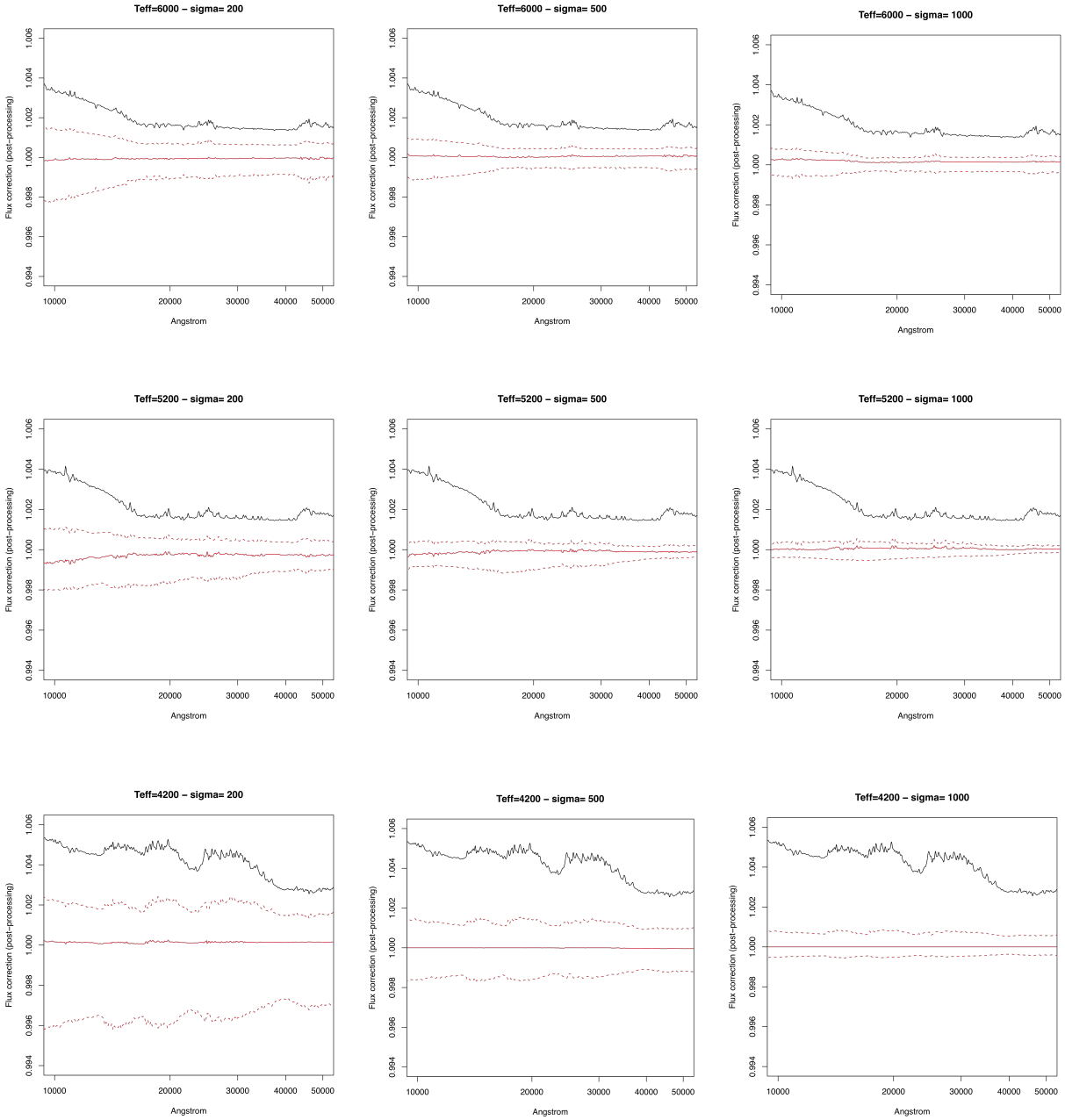

Figure 9: Spectrum distortion without corrections (solid black line), residual distortion after correction (median and 25 -75% percentiles of simulations).

4 NON-PARAMETRIC APPROACH: TREATING ACTIVITY AS "NOISE"

Non-parametric techniques have been used in a variety of astronomical contexts (e.g. Seikel et al. 2012; Chapman et al. 2013). In the exoplanet field in particular, these methods have been adopted by (e.g. Thatte et al. 2010; Gibson et al. 2012a; Ford et al. 2012; Waldmann 2012, 2013; Waldmann et al. 2013). Among these, the Gaussian Process (GP) method for regression (Rasmussen and Williams 2006), is widely used in the machine learning field and of increasing interest in the exoplanet community. GPs are defined as "non-parametric" as no parametric function is used to model the regression function (or classification boundary). The model indeed contains a covariance function and its parameters, but this function describes the properties of the regression function, rather than the regression function itself.

Danielski et al. (2013) have adopted a technique which uses GP-based methods to analyse the Kepler stellar light curves to extract the temporal events intrinsic to the stellar system, such as planetary transits or stellar flares. They repeated it on a sample of ten stars with different effective temperature, de-trending the short and long term stellar activity for each Kepler quarter. With the same approach they have also extrapolated the stellar flux in a simulated periodic monitoring scenario.

The method was successful to address two main issues:

1. Identifying clusters of outliers that are due to the astrophysical events, such as flares, planetary transits, occultations or general sudden variations in the intensity.
2. Iredicting the stellar flux at the 10^{-4} level in a situation where a constant monitoring of the star is not available.

The typical molecular features for a hot-Jupiter planet have a contrast of 1 part to 10^4 while for Super-Earths planets around a M dwarf star the contrast is 1 part on 10^4. Hence, the precision on the inferred planetary radius – and thus on the stellar activity correction, – needs to be of the same level. Whilst stellar activity can reveal itself in multiple ways, at first order approximation we can generalise it as a combination of two different timescales: a long and a short one. In the case of the Kepler data, the long term is ~90 days, while the lower limit, for both long- and short-term, corresponds to the integration time (~0.024 days). Depending on the causes of the stellar variation in each time-series these timescales will weight differently, and can be estimated measuring the power spectrum of the signal.

In a scenario of periodic observations that span different time intervals, Danielski and collaborators applied the GP-based method to predict the stellar flux where data are not available (Fig. 10). In the case of 10 hours of observations per day (for a total of 90 days) the extrapolated model is, on average, accurate at the 10^{-5} level compared to the one predicted using all the data available. When observations are sparser – e.g. 10 hours every second, third, fourth and fifth day – the accuracy of the stellar fit is ~10^{-4}. When data are taken for 10 hours every week, the accuracy drops to 10^{-3}. Table 5 shows these results for all

target. We notice that the accuracy of the fit also depends by the original noise standard deviation of the data.

Non parametric techniques can be a powerful tool to disentangle the planetary signal from the stellar activity noise. Given single time series on an active star with various modes of pulsation, obtained by the Kepler space telescope, a randomly chosen pulsation mode of the star can be isolated and the remaining autocorrelative noise of the star suppressed, resulting in a strong reduction of the stellar noise component (Waldmann 2012; Danielski et al. 2013). Non-parametric techniques can also be used to extrapolate the long term modulation of the stellar flux in a situation of non-continuous monitoring of the target. An accuracy of ~10^{-4} can be obtained even when data are recorded for ten hours every five days. This information is critical for EChO observations and in general for the studies of the atmospheres of exoplanets.

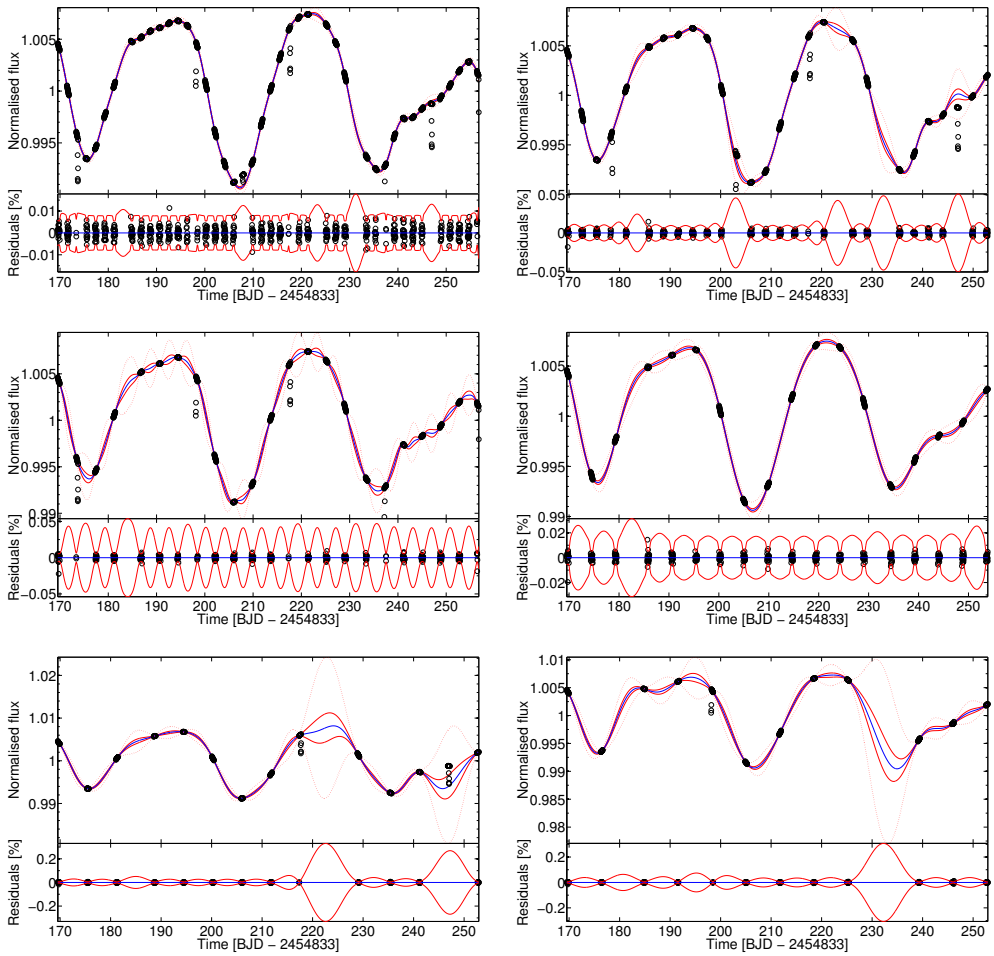

Figure 10: From left to right and from top to bottom: GP fit on all the data of KIC 10748390 (Q-2), on a set of 10 hours of observation per day, every second day, every third day, every fourth day, every fifth day, every sixth day and every week. The data are plot in black, the blue line represents the mean model, the red continuous and dotted line represent 1-σ and 5-σ uncertainty level (Danielski et al. 2013).

Targets					
KIC	T_{eff} [K]	R [$R_\odot$]	Kep_{mag}	Flag	ΔP [%]
3835670	5642	1.790	13.397	Planetary candidate	80.4 ± 20.3
2571238	5541	0.850	11.898	Exoplanet (Kepler-19b)	88.8 ± 11.7
6291653	5236	0.095	15.305	Planetary candidate	89.6 ±16
1026957	4917	0.788	12.559	False positive	–
7700622	4789	0.649	12.968	Planetary candidate	69.6 ±32.4
10748390	4766	0.058	9.147	Planetary candidate	28.5± 8.8
3128793	4668	0.637	14.633	Planetary candidate	70.9 ± 9.5
7603200	3900	0.612	12.925	Planetary candidate	81.4 ± 27.8
7907423	3803	0.492	15.234	Planetary candidate	89. ± 14.8
5080636	3673	0.024	14.404	Planetary candidate	38.3± 18.4

Accuracy of the extrapolated model [%]				
	3835670	6291653	7907423	7700622
10hr/1d	0.032	0.041	0.036	0.034
10hr/2d	0.037	0.046	0.045	0.036
10hr/3d	0.043	0.054	0.065	0.043
10hr/4d	0.046	0.058	0.068	0.044
10hr/5d	0.049	0.064	0.084	0.049
10hr/6d	0.055	0.069	0.102	0.062
10hr/7d	0.062	0.077	0.118	0.065
	10748390	5080636	3128793	7603200
10hr/1d	0.069	0.169	0.092	0.036
10hr/2d	0.075	0.056	0.132	0.045
10hr/3d	0.081	0.069	0.153	0.058
10hr/4d	0.084	0.069	0.158	0.064
10hr/5d	0.125	0.085	0.197	0.080
10hr/6d	0.124	0.102	0.302	0.103
10hr/7d	0.143	0.143	0.321	0.117

Table 5: Left: Table of the targets. For each target we report here the effective temperature (Teff), the stellar radius (Rd), the Kepler magnitude (Kmag), the flag as in the KOI catalogue and the variation on the most relevant period of the available quarters (ΔP). Right: Table of the average accuracy of the GP extrapolated model compared to the model fit on the complete light curve. The average has been measured over all the available long-cadence quarters in a scheme where 10 hours observation per day were selected, every second day, every third day, every fourth day, every fifth day, every sixth day and every week (Danielski et al. 2013).

5 REFERENCES

- Allard, F., Homeier, D., Freytag, B., Schaffenberger, W., & Rajpurohit, A. S., 2013, arXiv:1302.6559
- Ball, W. T., Unruh, Y. C., Krivova, N. A., Solanki, S., & Harder, J. W., 2011, A&A, 530, A71
- Ballerini, P., Micela, G., Lanza, A. F., Pagano, I., 2012, A&A, 539, A140
- Barros, S. C. C., Boué, G., Gibson, N. P., Pollacco, D. L., Santerne, A., Keenan, F. P., Skillen, I., & Street, R. A., 2013, MNRAS, 430, 3032
- Basri, G., Walkowicz, L., Reiners, A., 2013, ApJ, 769, id. 37
- Berdyugina, S. V., 2005, LRSP, 2, 8
- Dumusque, X., Santos, N. C., Udry, S., Lovis, C. & Bonfils, X., 2011a, A&A, 276, 527
- Dumusque, X., Lovis, C., Udry, S., & Santos, N. C., 2011b, A&A, 276, 530
- Fontenla, J. M., Curdt, W., Haberreiter, M., & Harder, J., Tian, H., 2009, ApJ, 707, 482
- Kipping, D. M., 2012, MNRAS, 427, 2487
- Lanza, A. F., Rodonò, M., Pagano, I., Barge P., & Llebaria, A., 2003, A&A, 403, 1135
- Moulds, V. E., Watson, C. A., Bonfils, X., Littlefair, S. P., & Simpson, E. K., 2013, MNRAS, 430, 1709

– Ortiz, A., Solanki, S. K., Domingo, V., Fligge, M., & Sanahuja, B., 2002, A&A, 388, 1036
– Waldmann, I.P., 2012, ApJ, 747, 12
–